Effect of Geometrical Parameters of H-Plane Conductive Diaphragm on the Behavior of a Rectangular Waveguide

Mohsen Kalantari [1•]

***Abstract*— In this paper, the modal analysis is used to study the behavior of a rectangular waveguide loaded with a transversely thin conductive discontinuity. To this end, a function must be made according to the geometry of discontinuity. This function is utilized instead of applying boundary conditions on the plane where the discontinuity is. This equation includes all the necessary boundary conditions simultaneously. The scattering parameters of the structure are related to the coefficients of the Fourier series of the newly defined function. Then, the return loss and insertion loss of different structures are investigated while the geometrical parameters of discontinuity take different values. The behavior of structures can be explained by how dense the coefficients of the Fourier series are. The simulation results show that the error of this technique is less than 2%. This analysis can enable designers to understand how the geometrical parameters of discontinuity affect the scattering parameters for an H-plane inductive diaphragm.**

***Index Terms*— Inductive diaphragm, Mode matching method, Rectangular waveguide.**

I. INTRODUCTION

WAVEGUIDES are vital components in telecommunication systems, especially for high-power transferring. They also play an important role in designing different microwave devices such as filters, couplers, duplexers, and circulators [1]-[9]. The operation of these devices is dependent on the existence of different discontinuities, such as the existence of posts and diaphragm in the waveguide, bend, and step change discontinuity [7]-[10]. Reference [11] points out a practical technique to determine the permittivity and loss tangent of a lossy dielectric. This technique requires inserting a sample of the desired material inside the resonant cavity. Authors in [11] utilize a discontinuity to improve the output power of the resonant cavity. This is one of many that demonstrates the important role of discontinuity in a reasonable manner.

Understanding the behavior of discontinuity in the waveguide is an important issue for microwave engineers. There are a lot of publications about the effect of discontinuity in the waveguide. In the following some of the related publications is provided.

In [12], different thin and thick junctions and diaphragms are analyzed. The accuracy of the method used to determine the transverse electromagnetic fields is discussed in this reference. The behavior of arbitrarily-shape discontinuities in rectangular waveguide is presented in [13]. Authors in [14] propose a dumbbell-shaped discontinuity loaded transversely on a waveguide. Also, a narrow-thickness band-pass filter is designed by cascading three of these discontinuities [14].

Discontinuities in the aforementioned cases are conductive. Authors in [15] apply a new technique to analyze inductive obstacles in arbitrary shapes, either metallic or dielectric. Their study is performed for discontinuities in rectangular waveguides. Discussions about the calculation of the scattering parameters for different posts, circular junctions, and corners in rectangular waveguides are presented in [16]. Reference [17] utilizes an integral equation to analyze the H-plane obstacles in a rectangular waveguide. Their analysis includes metallic obstacles or anything made of dielectric. This method is used by authors in [18] to study the behavior of inductive waveguide microwave components. They propose the Fast Multipole Method for large problems. Similarly, the integral equation in the spatial domain is used by [19] to analyze step discontinuity in waveguide in the presence of posts near discontinuity.

A hybrid technique is applied for the dielectric resonator in [20]. A combination of Mode Matching and Multimode Contour Integral is employed by authors to show how the H-plane dielectric post affects the behavior of the rectangular waveguide. In [21], authors use the Mode Matching method with the Fourier transform technique to analyze the different types of rectangular waveguide junctions.

Authors in [22] use the Finite Element Method (FEM) to determine the properties of a waveguide loaded by dielectric posts. Their proposed algorithm is in the direction of reducing the model order. Therefore, they show that this analysis can reduce the run time and storage. Moreover, reference [23] analyzes the waveguide components such as septum polarizer and ortho-mode transducer by FEM. In [24], authors employed a hybrid FEM and Mode Matching techniques to analyze waveguide filters.

An important section of these researches is the technique used to analyze the structure. Mode Matching method, Integral Equation, and FEM are used in above mentioned publications. Here are some other publications that determine the behavior of discontinuity by other numerical techniques. The Moment Method (MoM) is utilized by [10] to model currents that flow on different discontinuities. The discontinuities studied in [10] are some posts and diaphragms that are uniform in the direction parallel to the narrow side of a rectangular waveguide. Also, the authors determine the equivalent impedance for the discontinuity. Analysis of an inductively loaded waveguide is performed by utilizing the MoM-based Generalized Scattering Matrix (GSM) technique [25]. This analysis is developed so

1. Department of Electrical Engineering, Faculty of Engineering, Shahid Chamran University of Ahvaz, Ahvaz, Iran.
• Corresponding author Email: m.kalantari@scu.ac.ir

that it includes the dominant-mode region and double-mode region. The simulation results of some filters are presented in this article, too.

Analysis of mitered bends and capacitive posts in waveguide is performed using Boundary Integral-Resonant Mode Expansion (BI-RME) [26]. In [27], authors utilize the Boundary Condition Mode Matching (BCMM) method to obtain the behavior of both E-plane and H-plane bends in a rectangular waveguide. The Spectral-Element Method is the way that is utilized in [28] to extract the scattering parameters of E-plane stub and T-junction.

References [29] and [30] are two of the recent publications that include the discussion about discontinuity in waveguide. The author in [29] applies a technique based on the Mode Matching method to find the effect of the existence of bends in waveguide (curved waveguides). The applied methods in [30] are FEM and Mode Matching methods. The authors analyze a structure with rotational symmetry with the help of these techniques.

Since then, this manuscript has been devoted to the role of the geometrical properties on the reflection and transmission coefficients for a rectangular waveguide loaded with a transversely metallic diaphragm. A discussion about a proposed numerical method is given in the next section. This method is based on the Mode Matching technique, and the boundary conditions are applied through an equation. The geometrical parameters of the discontinuity reflect on the functions available in this equation. The simulation results are presented in Section III. The discussion is focused on how geometrical parameters of an inductive diaphragm can change the behavior of the structure. This section is followed by conclusions, which is the final section.

II. Analysis of the Structure by Modal Analysis

As mentioned before, different methods like FEM, MoM, Mode Matching method are utilized for analyzing the behavior of discontinuity in the waveguide. In this paper, the Mode Matching method is used to study the behavior of transverse discontinuity in the waveguide.

As shown in Fig. 1, discontinuity in a rectangular waveguide divides the inner waveguide space into two mediums, Medium I and Medium II. The intersection of these mediums is a plane where two mediums have a common boundary. The discontinuity is on this plane. Since then, this common boundary is referred to as the discontinuity plane. The discontinuity is assumed to be a conductive diaphragm loaded transversely on the waveguide.

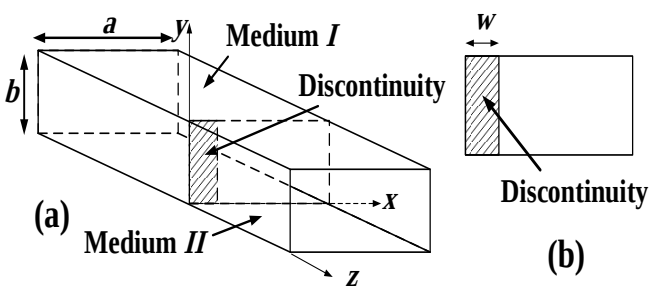

Fig. 1. (a) Transverse discontinuity in a rectangular waveguide, (b) front view. *a* and *b* are width and height of waveguide, respectively. *w* is the width of the diaphragm (discontinuity).

When an incident wave impinges on the discontinuity plane, some of the incident power is reflected from the discontinuity plane and accordingly forms the reflected wave. The remaining power passes through medium II (transmitted wave). According to Fig. 2, the reflected wave moves to the source, and the transmitted wave is propagated into the load.

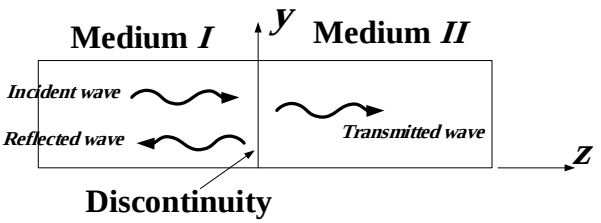

Fig. 2. Incident, reflected, and transmitted waves in the waveguide (side view)

In modal analysis, each electromagnetic field can be expanded in terms of different modes. Every mode is a nontrivial solution of the homogeneous Helmholtz equation. According to Fig. 2 and assuming that the structure is excited by the dominant mode (TE_{10}), relation (1) shows the expansion of the electric field of reflected and transmitted waves in terms of different modes [5], [7].

$$E_y^I = E_y^i + E_y^r \quad , \quad \begin{cases} E_y^i = \varphi_{10}(x,y)e^{-j\beta_{10}z} \\ E_y^r = \sum_m \sum_n a_{mn}\varphi_{mn}(x,y)e^{j\beta_{mn}z} \end{cases}$$
$$E_y^{II} = E_y^t \quad , \quad E_y^t = \sum_m \sum_n b_{mn}\varphi_{mn}(x,y)e^{-j\beta_{mn}z} \tag{1}$$

The superscripts *i*, *r*, and *t* represent the incident, reflected, and transmitted waves, respectively. $\varphi_{mn}(x,y)$ is the mode *mn*, and it is noted that each mode indicates the transverse variation of electromagnetic fields. The indices *m* and *n* determine the order of each mode. In (1), the phase constant for mode *mn* is shown by β_{mn}.

The coefficient of each mode (a_{mn} or b_{mn}) will be obtained by applying the boundary conditions on both sides of the discontinuity plane. These boundary conditions are as follows: the transverse electric fields are equal to zero on the metal region of the discontinuity plane, and the transverse components of electric and magnetic fields have to be continuous on other sections. It means that [7];

$$E_t^I = \begin{cases} 0 & on\ R \\ E_t^{II} & on\ R^c \end{cases} \qquad H_t^I = \begin{cases} |\vec{J}_-| & on\ R \\ H_t^{II} & on\ R^c \end{cases} \tag{2}$$

Where *R* is a conductive region of discontinuity plane, and R^c is the complementary part of *R* on the discontinuity plane. According to Fig. 1, *R* refers to discontinuity, and R^c is the window between two mediums. The $\vec{J}_-$ refers to the density of surface current flows on the discontinuity plane in medium I. Subscript *t* is used to show tangential component of $\vec{E}$ and $\vec{H}$.

References [31] and [32] propose a new equation instead of applying the above boundary conditions for metal grid structures. This work is followed by [33] to determine the behavior of a metasurface. Later, Reference [34] extends this work to analyze any inductive diaphragm in rectangular waveguide [31]-[32], [34].

$$f(x,y)E_t^I + g(x,y)(H_t^I - H_t^{II}) = 0 \tag{3}$$

$$f(x,y)\begin{cases}\neq 0 & on\ R\\ =0 & on\ R^c\end{cases} \quad \& \quad g(x,y)\begin{cases}=0 & on\ R\\ \neq 0 & on\ R^c\end{cases}$$

Equation (3) will be considered as the cornerstone of the following calculation. In reality, functions $f(x,y)$ and $g(x,y)$ are made to simplify applying boundary conditions on the discontinuity plane. It can be said that these functions represent the boundary conditions. Therefore, they are Boundary-Conditions Equivalent (BCE) or Boundary-Conditions Alternative (BCA) functions.

It should be noted that the zero tangential electric field is required at the discontinuity plane when using Equation (3). Also, zero thickness is assumed for discontinuity. Waveguides are known to be made from metal, and this also applies to the discontinuity mentioned in this paper. According to [33], the thickness of metallic discontinuity should be larger than 5 skin depths. On the other hand, the thickness should be less than the wavelength, so the variation of fields is negligible on both sides of the discontinuity plane (R^c).

For frequencies in which the dominant mode is the only mode propagated in the waveguide, all higher-order modes are evanescent and should vanish when they move away from the discontinuity. Therefore, the amplitude of the dominant mode determines the behavior of the structure. Since many of these modes are non-propagating modes, the excitation of these modes causes energy concentration in the waveguide [7].

As shown in Fig. 1, if the discontinuity is uniform in the *y*-direction, only TE_{m0} modes are excited in the waveguide [7]. It means that no TE_{mn} ($n \neq 0$) modes are excited, and the electromagnetic fields are dependent only on variable *x*. Therefore, the electromagnetic fields of incident, reflected, and transmitted waves can be written as (4) and (5) [7].

$$E_y^i=sin\left(\frac{\pi}{a}x\right)e^{-j\beta_{10}^I z},\ E_y^r=\sum_{m=1}^{\infty} a_m sin\,(m\frac{\pi}{a}x)e^{j\beta_{m0}^I z} \qquad E_y^t=\sum_{m=1}^{\infty} b_m sin\,(m\frac{\pi}{a}x)e^{-j\beta_{m0}^{II} z} \tag{4}$$

$$H_x^i=\frac{-1}{Z_{10}^I}\sin\,(\frac{\pi}{a}x)e^{-j\beta_{10}^I z},\quad H_x^r=\sum_{m=1}^{\infty}\frac{a_m}{Z_{m0}^I}\sin\,(m\frac{\pi}{a}x)e^{j\beta_{m0}^I z} \qquad H_x^t=\sum_{m=1}^{\infty}\frac{-b_m}{Z_{m0}^{II}}\sin\,(m\frac{\pi}{a}x)e^{-j\beta_{m0}^{II} z} \tag{5}$$

Where the superscripts *i*, *r*, and *t* represent the incident, reflected, and transmitted waves, respectively. As seen in the above equations, the transverse variation of electromagnetic fields is represented by $sin(m\pi x/a)$ for TE_{m0} modes. Z_{m0} and β_{m0} are the characteristic impedance and phase constant for mode *m*0, respectively. Also, the superscripts *I* and *II* refer to medium I and medium II, respectively. Equation (6) shows how Z_{m0} and β_{m0} are calculated [7].

$$\beta_{m0}=\sqrt{\omega^2\mu\varepsilon-\left(m\frac{\pi}{a}\right)^2} \quad , \quad Z_{m0}=\frac{\omega\mu}{\beta_{m0}} \tag{6}$$

In (6), ω is angular frequency, and a is the width of the waveguide (Fig. 1). The parameters ε and μ are permittivity and permeability of medium, respectively.

Since the electromagnetic fields ((4) and (5)) are *x*-dependent and the structure is uniform in the *y*-direction, (3) simplifies to (7) [31]-[32], [34].

$$f(x)E_t^I+g(x)(H_t^I-H_t^{II})=0 \tag{7}$$

By substituting (4) and (5) in (7), (8) is derived (Appendix A).

$$f(x)\left\{\sum_{m=1}^{\infty}\{a_m+\delta_{m1}\}sin\,(\frac{m\pi}{a}x)\right\}+ g(x)\left\{\sum_{m=1}^{\infty}2\frac{a_m}{Z_{m0}}sin\,(\frac{m\pi}{a}x)\right\}=0 \tag{8}$$

Where δ_{m1} is Kronecker delta. To obtain (8), it is assumed that the two mediums, medium I and medium II, are the same. It must be noted that the BCA functions are not dependent on *y* due to the uniformity of discontinuity in *the y*-direction. Hence, functions $f(x,y)$ and $g(x,y)$ appear as $f(x)$ and $g(x)$ in (8), respectively. Equation (8) is utilized to simulate different inductive diaphragms in the next section. Functions $f(x)$ and $g(x)$ are created according to (3). The geometry of the discontinuity prominently affects the definition of BCA functions. In the next step, it is possible to determine f_ks and g_ks, the coefficients of the Fourier series of functions $f(x)$ and $g(x)$ (Appendix A). Having f_ks and g_ks, the coefficient of each mode is obtained by (8) (Fig. 3). The scattering parameters for the structure can be achieved by these coefficients. In the following section, the main goal is to investigate the effects of the width and position of discontinuity on the behavior of a structure.

Step 1: Make BCA functions, $f(x)$ and $g(x)$, based on geometry of discontinuity

→ Step 2: Determine f_ks and g_ks, the coefficients of Fourier series for $f(x)$ and $g(x)$

→ Step 3: Obtain scattering parameters

Fig. 3. The successive steps for obtaining the scattering parameters of a metallic discontinuity loaded transversely in the waveguide.

III. Simulation Results

In this section, the simulation results for different discontinuities are presented. As given in Fig. 1, it is assumed that the discontinuity is a metallic septum loaded transversely on a rectangular waveguide. The simulated rectangular waveguide is *WR*90, while its width and height are 22.86 *mm* and 10.16 *mm*, respectively. The cutoff frequency for this waveguide is 6.56 *GHz*. For each simulation, 150 modes are considered.

The first discontinuity to be simulated is a 5 *mm*-width diaphragm. There is no gap between the diaphragm and the waveguide wall (Fig. 4). Simulation results for this structure are illustrated for two sets of BCA functions, namely $f_i(x)$ and $g_i(x)$ (9).

$$f_1(x)=\begin{cases}1 & 0<x<w\\ 0 & w<x<a\end{cases},\quad g_1(x)=\begin{cases}0 & 0<x<w\\ 1 & w<x<a\end{cases}$$
$$f_2(x)=\begin{cases}\sin\left(\pi\frac{x}{w}\right) & 0<x<w\\ 0 & w<x<a\end{cases},\quad g_2(x)=\begin{cases}0 & 0<x<w\\ \sin\left(\pi\frac{x-w}{a-w}\right) & w<x<a\end{cases} \tag{9}$$

Where *a* and *w* are 22.86 *mm* and 5 *mm*, respectively.

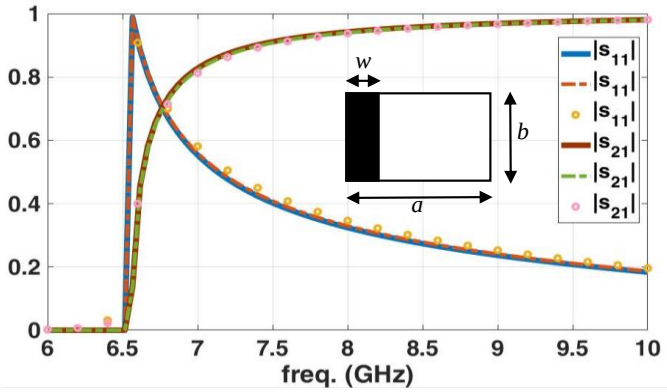

Fig. 4. The frequency variation of the scattering parameters for a diaphragm connected to waveguide wall. Solid blue: $|s_{11}|$ simulated when BCA functions are $f_1(x)$ and $g_1(x)$, red dashed line: $|s_{11}|$ simulated when BCA functions are $f_2(x)$ and $g_2(x)$, orange circles: $|s_{11}|$ simulated by FEM, Solid brown: $|s_{21}|$ simulated when BCA functions are $f_1(x)$ and $g_1(x)$, green dashed line: $|s_{21}|$ simulated when BCA functions are $f_2(x)$ and $g_2(x)$, and pink circles: $|s_{21}|$ simulated by FEM.

To verify the results obtained by modal analysis, the structure is simulated by FEM, and the simulation results are added to Fig. 4. As shown in Fig. 4, the simulation results are in compliance to each other. The variation of the total electric field on the transverse plane is shown in Fig. 5.

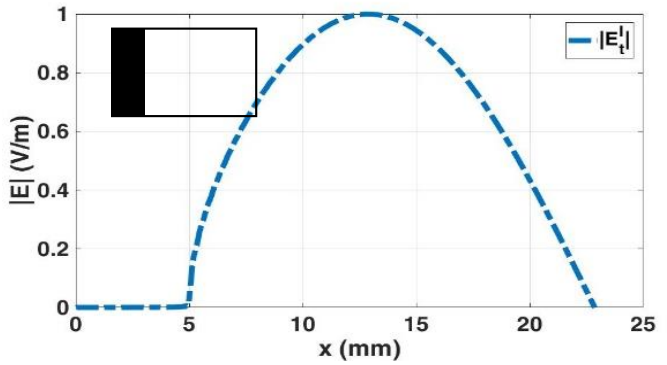

Fig. 5. The variation of total electric field ($\vec{E}_y^i + \vec{E}_y^r$) on the transverse plane. The maximum value of the transverse electric field is considered to be 1. It must be noted that there is no longitudinal component of the electric field for the TE_{mn} modes. Therefore, the total electric field is the transverse component of the electric field.

From this point on, BCA functions $f_1(x)$ and $g_1(x)$ are used to analyze the structures.

In Fig. 6, the variations of $|s_{11}|$ are shown so that the diaphragm moves from the waveguide wall to the center of the transverse plane. For all the values of g, the width of the diaphragm (w) is fixed to 5.45 *mm*. The readers must be aware of g and $g(x)$. g is the parameter that indicates the gap between the diaphragm and waveguide wall (Fig. 6), and $g(x)$ is the function that is needed for constructing (8).

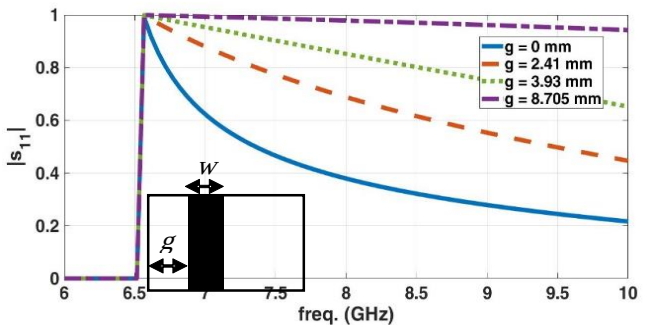

Fig. 6. The frequency variation of $|s_{11}|$ for different values of gap (g), which is the distance between waveguide wall and discontinuity. The parameter g is increased from 0 to 8.705 *mm* (= a/2-w/2). w is equal to 5.45 *mm* for all values of g.

As shown in Fig. 6, all curves for $|s_{11}|$ are strictly descending but with different rates. The more the diaphragm is close to the waveguide wall, the more rapidly $|s_{11}|$ tends to decrease. Unlike the $|s_{11}|$, each curve for $|s_{21}|$ follows a strictly ascending regime (Fig. 7). Equation (10) complies with this behavior. Since the structure is lossless and passive, incident power is divided between reflected and transmitted powers [7].

$$|s_{11}|^2+|s_{21}|^2=1 \rightarrow \quad 2|s_{11}|\frac{d|s_{11}|}{df}+2|s_{21}|\frac{d|s_{21}|}{df}=0$$
$$\rightarrow \frac{d|s_{21}|}{df}=-\frac{d|s_{11}||s_{11}|}{df \quad |s_{21}|} \tag{10}$$

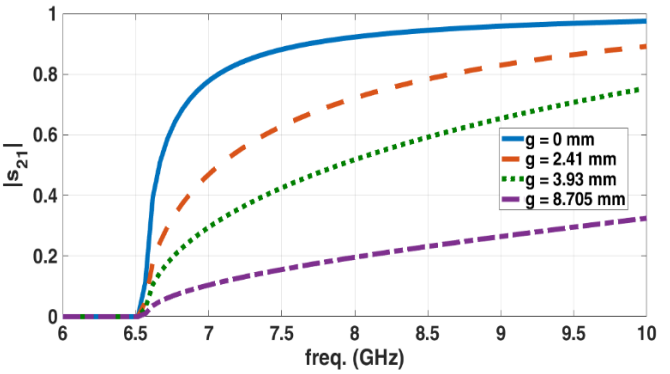

Fig. 7. The frequency variation of $|s_{21}|$ for different values of the gap (g). w is constant (w = 5.45 *mm*) in all cases.

Fig. 8 demonstrates the coefficients of the Fourier series for BCA function $f(x)$.

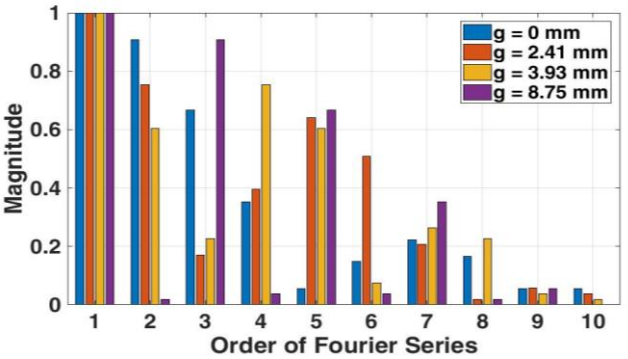

Fig. 8. The first 10 coefficients of the Fourier series for $f(x)$, (f_k , k = 1, 2, …, 10), versus increasing the gap (g).

The quantitative values are also given in Table. I for keen readers who want to have access to exact component values.

TABLE I

The First 10 Coefficients of the Fourier Series for $f(x)$, (f_k , k = 1, 2, …, 10), Versus Increasing the Gap (g) Between the Diaphragm and Waveguide Wall (w = 5.45 *mm* for all cases).

g(mm)	**0**	**2.41**	**3.93**	**8.705**
f_1	1	1	1	1
f_2	0.9074	0.7547	0.6038	0.0185
f_3	0.6667	0.1698	0.2264	0. 9074
f_4	0.3519	0.3962	0. 7547	0.0370
f_5	0.0556	0.6415	0.6038	0. 6667
f_6	0.1481	0.5094	0.0775	0.0370
f_7	0.2222	0.2075	0.2642	0.3519
f_8	0.1667	0.0189	0.2264	0.0185
f_9	0.0556	0.0556	0.0377	0.0566
f_{10}	0.0556	0.0377	0.0189	0.0000

Considering Fig. 6 and Table I. Simultaneously, the first coefficient of $f(x)$, f_1, is the same for all values of g due to the constant width of the diaphragm. When the diaphragm is further away from the waveguide wall, the second biggest coefficient of the Fourier series of $f(x)$ dislocates to the position of higher order components. Simultaneously, $|s_{11}|$ tends to decrease at a slower pace. Investigation of higher coefficients of BCA function $f(x)$ reveals that the modes with greater magnitudes are concentrated to the first mode (f_1) when g approaches zero. It is clear that increasing the gap, from $a/2$-$w/2$ to a-w, leads to the repetition of the above results in the reverse manner.

In Fig. 9, the variation of $|s_{11}|$ is shown while the diaphragm width increases. The parameter w starts from 3.57 *mm* and reaches 14.29 *mm* when there is no gap between discontinuity and waveguide wall (g = 0 *mm*).

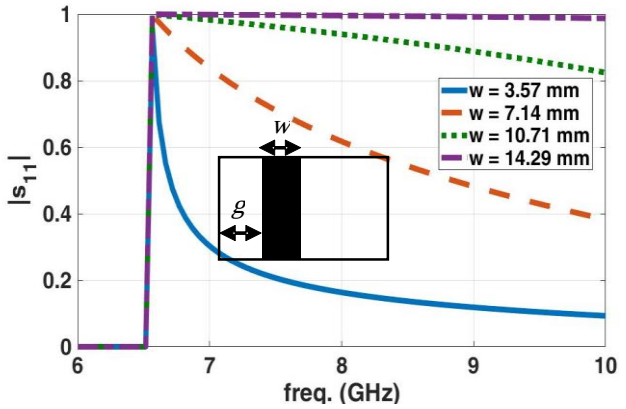

Fig. 9. The frequency variation of $|s_{11}|$ for different values of width (w), (g = 0 *mm*).

The narrower the diaphragm, the magnitude of s_{11} ($|s_{11}|$) tends to decrease more rapidly to the final value. On the contrary, the variation of parameter $|s_{21}|$ is in an ascending manner (Fig. 10). Growth of the parameter $|s_{21}|$ to the final value occurs in a narrower bandwidth as w becomes smaller.

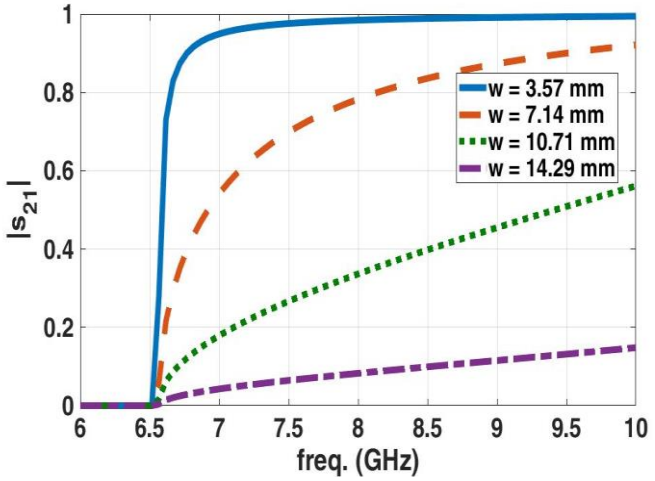

Fig. 10. The frequency variation of $|s_{21}|$ for different values of the width of the diaphragm (w), (g = 0 *mm*).

It is known that the designers model this discontinuity as a parallel reactance (jX) in the middle of a transmission line [4]-[8]. Table II contains the equivalent reactance for the diaphragm at 7 GHz. It connects to the waveguide wall, and its width is available in the table (Fig. 9).

TABLE II
The Equivalent Reactance (Ω) for H-plane Asymmetric Diaphragm at 7 *GHz* (g = 0 *mm* for all cases).

w(mm)	**3.57**	**7.14**	**10.71**	**14.29**
Ref. [6]	1656.7	346.4	98.2	23.1
Proposed technique	1685	347	98.7	23
Error (%)	1.71	0.17	0.51	0.43

The 2nd row is filled by the relation available in [6]. The values in the 3rd row are obtained by the scattering parameters shown in Fig. 9. It is clear that the 3rd row follows the 2nd row very well. The table's last row demonstrates that the error is less than 2% for the proposed technique. This means that the proposed technique has acceptable accuracy.

The first 10 coefficients of the Fourier series for BCA function $f(x)$ are shown in Fig. 11. Also, the quantitative values are given in Table. III. Note that all coefficients are normalized to the f_1, the first component of $f(x)$ for each value of g. According to (3), f(x) must be non-zero on R. Therefore, we consider factor p for each case so that the f_1 is equal to 1.

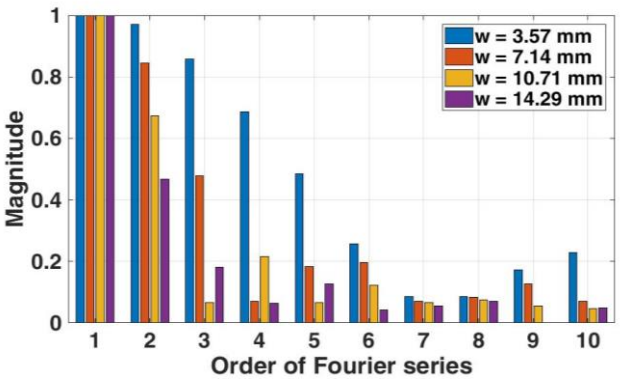

Fig. 11. The first 10 coefficients of the Fourier series for $f(x)$, (f_k , k = 1, 2, …, 10), versus increasing the width of the diaphragm (w) (g= 0 *mm* for all cases).

TABLE III
The First 10 Coefficients of the Fourier Series for $f(x)$ Versus the Width (w) of the Diaphragm (g = 0 *mm*).

w(mm)	**3.57**	**7.14**	**10.71**	**14.29**
f_1	1	1	1	1
f_2	0.9714	0.8451	0.6729	0.4685
f_3	0.8571	0.4789	0.0654	0.1818
f_4	0.6857	0.0704	0.2150	0.0629
f_5	0.4857	0.1831	0.0654	0.1259
f_6	0.2571	0.1972	0.1215	0.0420
f_7	0.0857	0.0704	0.0654	0.0559
f_8	0.0857	0.0845	0.0748	0.0699
f_9	0.1714	0.1268	0.0561	0.0000
f_{10}	0.2286	0.0704	0.0467	0.0490

Fig. 9 and Table. III show that as w increases, the magnitude of s_{11} ($|s_{11}|$) decreases more slowly. The biggest coefficient of the Fourier series happens for k = 1 for each case. The second biggest coefficient moves away from the first one when w increases. Same as the previous case, integration of the coefficients with higher magnitude around f_1 leads to a faster rate for the variation of scattering parameters in frequency domain.

The above examples show how the equation (3) and BCA functions are used to determine the scattering parameters of H-plane discontinuities. This equation can be used to predict the behavior of E-plane discontinuities. It requires considering all TE_{mn} and TM_{mn} modes excited in the rectangular waveguide. We certainly encounter more processes, two-dimensional diagrams for components of BCA functions, and so on. Reference [33] shows how this equation applies to a TEM waveguide where all TEM, TE, and TM modes are excited around an element of a metasurface.

IV. Conclusion

In this paper, the dependency of reflection and transmission coefficients on geometrical parameters for the inductive diaphragm is discussed. The simulation of the structure is performed by modal analysis. In this way, boundary conditions on both sides of discontinuity are applied by an equation. Two BCA functions must be defined to make this equation. Considering the components of the Fourier series of the BCA function indicates that the concentration of bigger components around the first-order component is an effective factor in determining the behavior of the structure. The error of this technique is considered by simulation. It is less than 2%. This analysis hints at the relation between the geometrical parameters of structure and its reflection and transmission coefficients. Also, it can lead to a better understanding of the behavior of the structure. This method can be a part of an optimization algorithm to find the final solution faster.

V. Appendix A

Appendix A clarifies how to derive (8). According to (2), the tangential component of electric fields in medium I is zero on R, and it is equal to the tangential component of electric fields in medium II on R^c. Simultaneously, this condition is valid for the tangential component of electric fields in medium II.

$$E_t^{II} = \begin{cases} 0 & on\ R \\ E_t^I & on\ R^c \end{cases} \quad (A.1)$$

It means that the tangential components of the electric field are continuous on the discontinuity plane.

$$E_t^I = E_t^{II} \quad \rightarrow \quad \sin\left(\frac{\pi}{a}x\right) + \sum_{m=1}^{\infty} a_m \sin\left(\frac{m\pi}{a}x\right) = \sum_{m=1}^{\infty} b_m \sin\left(\frac{m\pi}{a}x\right) \quad \rightarrow \quad b_m = a_m + \delta_{m1} \quad (A.2)$$

Other Boundary conditions are applied using (8);

$$f(x)E_t^I + g(x)(H_t^I - H_t^{II}) = 0 \quad (A.3)$$

Now, using (4) and (5),

$$f(x)\left\{\sum_{m=1}^{\infty}\{a_m + \delta_{m1}\}\sin\left(\frac{m\pi}{a}x\right)\right\} + g(x)\left\{\sum_{m=1}^{\infty}\left[\left(\frac{1}{Z_{m0}^I} + \frac{1}{Z_{m0}^{II}}\right)a_m + \left(\frac{1}{Z_{m0}^{II}} - \frac{1}{Z_{m0}^I}\right)\delta_{m1}\right]\sin\left(\frac{m\pi}{a}x\right)\right\} = 0 \quad (A.4)$$

Rearranging the above relation;

$$\left\{\sum_{m=1}^{\infty} a_m f(x) sin\left(\frac{m\pi}{a}x\right)\right\} + \left\{\sum_{m=1}^{\infty}\left[\left(\frac{1}{Z_{m0}^I} + \frac{1}{Z_{m0}^{II}}\right)a_m g(x)\right] sin\left(\frac{m\pi}{a}x\right)\right\} = -f(x) sin\left(\frac{\pi}{a}x\right) + \left[\left(\frac{1}{Z_{10}^I} - \frac{1}{Z_{10}^{II}}\right)g(x)\right] sin\left(\frac{\pi}{a}x\right) \quad (A.5)$$

Multiplying two sides of the above relation in the function $sin(k\pi x/a)$, and taking integral on $[0,a]$;

$$\left\{\sum_{m=1}^{\infty} a_m\left[\int_0^a f(x) sin\left(\frac{m\pi}{a}x\right) sin\left(\frac{k\pi}{a}x\right)dx\right]\right\} + \left\{\sum_{m=1}^{\infty}\left(\frac{1}{Z_{m0}^I} + \frac{1}{Z_{m0}^{II}}\right)a_m\left[\int_0^a g(x) sin\left(\frac{m\pi}{a}x\right) sin\left(\frac{k\pi}{a}x\right)dx\right]\right\} = -\int_0^a f(x) sin\left(\frac{\pi}{a}x\right) sin\left(\frac{k\pi}{a}x\right)dx + \left(\frac{1}{Z_{10}^I} - \frac{1}{Z_{10}^{II}}\right)\left[\int_0^a g(x) sin\left(\frac{\pi}{a}x\right) sin\left(\frac{k\pi}{a}x\right)dx\right] \quad (A.6)$$

By considering that $sin(m\pi x/a)sin(k\pi x/a) = 0.5\{cos[(k-m)\pi x/a] - cos[(k+m)\pi x/a]\}$;

$$\left\{\sum_{m=1}^{\infty} a_m\left[\int_0^a f(x)\cos\left[(k-m)\frac{\pi}{a}x\right]dx - \int_0^a f(x)\cos\left[(k+m)\frac{\pi}{a}x\right]dx\right]\right\} + \left\{\sum_{m=1}^{\infty}\left(\frac{1}{Z_{m0}^I} + \frac{1}{Z_{m0}^{II}}\right)a_m\left[\int_0^a g(x)\cos\left[(k-m)\frac{\pi}{a}x\right]dx - \int_0^a g(x)\cos\left[(k+m)\frac{\pi}{a}x\right]dx\right]\right\} = \left[\int_0^a f(x)\cos\left[(1+k)\frac{\pi}{a}x\right]dx - \int_0^a f(x)\cos\left[(1-k)\frac{\pi}{a}x\right]dx\right] + \left(\frac{1}{Z_{10}^{II}} - \frac{1}{Z_{10}^I}\right)\left[\int_0^a g(x)\cos\left[(1+k)\frac{\pi}{a}x\right]dx\right] + \left(\frac{1}{Z_{10}^I} - \frac{1}{Z_{10}^{II}}\right)\left[\int_0^a g(x)\cos\left[(1-k)\frac{\pi}{a}x\right]dx\right] \quad (A.7)$$

Rearranging this relation;

$$\sum_{m=1}^{\infty} a_m f_{m-k} - \sum_{m=1}^{\infty} a_m f_{m+k} + \sum_{m=1}^{\infty}\left(\frac{1}{Z_{m0}^{II}} + \frac{1}{Z_{m0}^I}\right)a_m g_{m-k} - \sum_{m=1}^{\infty}\left(\frac{1}{Z_{m0}^{II}} + \frac{1}{Z_{m0}^I}\right)a_m g_{m+k} = f_{1+k} - f_{1-k} + \left(\frac{1}{Z_{10}^{II}} - \frac{1}{Z_{10}^I}\right)g_{1+k} + \left(\frac{1}{Z_{10}^I} - \frac{1}{Z_{10}^{II}}\right)g_{1-k} \quad (A.8)$$

By truncating each sum at N and taking k from 0 to N, a system is obtained;

$$(A - B + CZ - DZ)\begin{bmatrix} a_1 \\ a_1 \\ a_1 \\ \vdots \\ a_N \end{bmatrix} = E - F + \left(\frac{1}{Z_{10}^{II}} - \frac{1}{Z_{10}^I}\right)G + \left(\frac{1}{Z_{10}^I} - \frac{1}{Z_{10}^{II}}\right)H \quad (A.9)$$

Where A, B, C, and D are matrices with size $N\times N$.

$$A = \begin{bmatrix} f_0 & f_1 & f_2 & \cdots \\ f_{-1} & f_0 & f_1 & \cdots \\ f_{-2} & f_{-1} & f_0 & \cdots \\ & \vdots & & \end{bmatrix},\ B = \begin{bmatrix} f_2 & f_3 & f_4 & \cdots \\ f_3 & f_4 & f_5 & \cdots \\ f_4 & f_5 & f_6 & \cdots \\ & \vdots & & \end{bmatrix},\ C = \begin{bmatrix} g_0 & g_1 & g_2 & \cdots \\ g_{-1} & g_0 & g_1 & \cdots \\ g_{-2} & g_{-1} & g_0 & \cdots \\ & \vdots & & \end{bmatrix},\ D = \begin{bmatrix} g_2 & g_3 & g_4 & \cdots \\ g_3 & g_4 & g_5 & \cdots \\ g_4 & g_5 & g_6 & \cdots \\ & \vdots & & \end{bmatrix} \quad (A.10)$$

Matrix Z is a diagonal matrix with size $N\times N$. The elements of this matrix are frequency-dependent. Also, they are dependent on characteristic parameters of the medium (ε and μ).

$$Z = \begin{bmatrix} \left(\frac{1}{Z_{10}^{II}} + \frac{1}{Z_{10}^I}\right) & 0 & 0 & \cdots \\ 0 & \left(\frac{1}{Z_{20}^{II}} + \frac{1}{Z_{20}^I}\right) & 0 & \cdots \\ 0 & 0 & \left(\frac{1}{Z_{30}^{II}} + \frac{1}{Z_{30}^I}\right) & \cdots \\ & & \vdots & \end{bmatrix} \quad (A.11)$$

And E, F, G, and H are matrices with size $N\times 1$.

$$E = \begin{bmatrix} f_2 \\ f_3 \\ f_4 \\ \vdots \end{bmatrix},\ F = \begin{bmatrix} f_0 \\ f_{-1} \\ f_{-2} \\ \vdots \end{bmatrix},\ G = \begin{bmatrix} g_2 \\ g_3 \\ g_4 \\ \vdots \end{bmatrix},\ H = \begin{bmatrix} g_0 \\ g_{-1} \\ g_{-2} \\ \vdots \end{bmatrix} \quad (A.12)$$

VI. Acknowledgment

This work was supported in part by Shahid Chamran University of Ahvaz under Grant SCU.EE1402.73363. The author thanks Dr. Ehsan Namjoo for his great help and guidance in the writing of this paper.

VII. REFERENCES

[1] C. A. Balanis, "Advanced Engineering Electromagnetics", Wiley, 2012.

[2] R. F. Harrington, "Time-Harmonic Electromagnetic Fields", IEEE Press Series on Electromagnetic Wave Theory, Wiley, 2001.

[3] M. N. O. Sadiku, "Numerical Techniques in Electromagnetics with MATLAB", CRC Press, 2018.

[4] R. E. Collin, "Field Theory of Guided Wave", IEEE Press Series on Electromagnetic Wave Theory, Wiley, 1990.

[5] T. Itoh, "Numerical Techniques for Microwave and Millimeter-Wave Passive Structures", Wiley, 1989.

[6] N. Marcuvitz, "Waveguide Handbook", The Institution of Engineering and Technology, 1986.

[7] D. M. Pozar, "Microwave Engineering", John wiley & sons, 2011.

[8] G. L. Matthaei, L. Young, E. M. T. Jones, "Microwave filters, impedance-matching networks, and coupling structures", Artech House, Norwood, 1980.

[9] I. Hunter, "Theory and Design of Microwave Filters' IEE electromagnetic waves series", Institution of Engineering and Technology, Institution of Electrical Engineers, 2001.

[10] H. Auda, R.F. Harrington, "Inductive Posts and Diaphragms of Arbitrary Shape and Number in a Rectangular Waveguide", *IEEE Transactions on Microwave Theory and Techniques*, vol. 32, no. 6, pp. 606-613, 1984.

[11] M. Karami, P. Rezaei, N. Bahari, "A modified rectangular resonant cavity utilizing frequency selective coupled end-plate for dielectric constant measurement by perturbation technique", *International Journal of RF and Microwave Computer-Aided Engineering*, vol. 32, no. 6, pp. 508-517, p.e23125, 2022.

[12] A. Wexler, "Solution of waveguide discontinuities by modal analysis", *IEEE Transactions on Microwave Theory and Techniques*, vol. 15, no. 9, pp. 508-517, 1967.

[13] R.H. MacPhie, Ke-Li Wu, "A full-wave modal analysis of arbitrarily shaped waveguide discontinuities using the finite plane-wave series expansion", *IEEE Transactions on Microwave Theory and Techniques*, vol. 47, no. 2, pp. 232-237, 1999.

[14] H. Hu, X. Lei, J. Wu, "Design of a compact dumbbell-shape twist waveguide with performance of band-pass filtering", 2017 IEEE 17th International Conference on Communication Technology (ICCT), 2017, Chengdu, China, pp. 1045-1048.

[15] H. Esteban, S. Cogollos, V.E. Boria, A.S. Blas, M. Ferrando, "A new hybrid mode-matching/numerical method for the analysis of arbitrarily shaped inductive obstacles and discontinuities in rectangular waveguides", *IEEE Transactions on Microwave Theory and Techniques*, vol. 50, no. 4, pp. 1219-1224, 2002.

[16] I.D. Stamatopoulos, I.D. Robertson, "Rigorous network representation of microwave components by the use of indirect mode matching", *IEEE Transactions on Microwave Theory and Techniques*, vol. 52, no. 3, pp. 935-944, 2004.

[17] F.D.Q. Pereira , V.E.B. Esbert, J.P. Garcia, A.V. Pantaleoni, A.A. Melcon, J.L.G. Tornero, B. Gimeno, "Efficient Analysis of Arbitrarily Shaped Inductive Obstacles in Rectangular Waveguides Using a Surface Integral-Equation Formulation", *IEEE Transactions on Microwave Theory and Techniques*, vol. 55, no. 4, pp. 715-721, 2007.

[18] F.P. Soler, F.Q. Pereira, J.P.-Garcia, D.C. Rebenaque, A.A. Melcon, "Analysis of Inductive Waveguide Microwave Components Using an Alternative Port Treatment and Efficient Fast Multipole", *Progress In Electromagnetics Research*, vol. 68, pp. 71-90, 2007.

[19] F.Q. Pereira, C.G. Molina, A.A. Melcon, V.E. Boria, M. Guglielmi, "Novel spatial domain integral equation formulation for the analysis of rectangular waveguide steps close to arbitrarily shaped dielectric and/or conducting posts", *Radio Science*, vol. 53, no. 4, pp. 406-419, 2018.

[20] A. Banai, A. Hashemi, "A hybrid multimode contour integral method for analysis of the H-plane waveguide discontinuities", *Progress In Electromagnetics Research*, vol. 81, pp. 167-182, 2008.

[21] H. Jia, K. Yoshitomi, K. Yasumoto, "Rigorous analysis of rectangular waveguide junctions by Fourier transform technique", *Progress In Electromagnetics Research*, vol. 20, pp. 263-282, 1998.

[22] G. Fotyga, K. Nyka, M. Mrozowski, "Efficient Model Order Reduction for FEM Analysis of Waveguide Structures and Resonators", *Progress In Electromagnetics Research*, vol. 127, pp. 277-295, 2012.

[23] G.G. Gentili, L. Accatino G. Bertin, "The Generalized 2.5-D Finite-Element Method for Analysis of Waveguide Components", *IEEE Transactions on Microwave Theory and Techniques*, vol. 64, no. 8, pp. 2392-2400, 2016.

[24] R. Beyer, F. Arndt, "Efficient modal analysis of waveguide filters including the orthogonal mode coupling elements by an MM/FE method", *IEEE Microwave and Guided Wave Letters*, vol. 5, no. 1, pp. 9-11, 1995.

[25] A. Aydogan, "An inclusive analysis of inductive dielectric and/or metallic discontinuities in a rectangular waveguide", *Microwave and Optical Technology Letters*, vol. 63, no. 2, pp. 383-392, 2021.

[26] S. Battistutta, M. Bozzi, M. Bressan, L. Perregrini, "Extension of the BI-RME method to the analysis of piecewise-homogeneous waveguide components including arbitrarily shaped building blocks", 2017 47th European Microwave Conference (EuMC), 2017, Nuremberg, Germany, 2017, pp. 884-887.

[27] J.M. Reiter, F. Arndt, "Rigorous analysis of arbitrarily shaped H- and E-plane discontinuities in rectangular waveguides by a full-wave boundary contour mode-matching method", *IEEE Transactions on Microwave Theory and Techniques*, vol. 43, no. 4, pp. 796-801, 1995.

[28] O.A. Peverini, G. Addamo, G. Virone, R. Tascone, R. Orta, "A Spectral-Element Method for the Analysis of 2-D Waveguide Devices With Sharp Edges and Irregular Shapes", *IEEE Transactions on Microwave Theory and Techniques*, vol. 59, no. 7, pp. 1685-1695, 2011.

[29] G.S. Rosa, "A Mode-Matching-Based Formulation for the Analysis of Curved Rectangular Waveguides", *IEEE Transactions on Microwave Theory and Techniques*, vol. 71, no. 9, pp. 3810-3818, 2023.

[30] G. Garcia-Contreras, J. Corcoles, J.A. Ruiz-Cruz. "Native 2-D-FEM/Mode-Matching Formulation for Second-Order Symmetric Waveguide Devices", *IEEE Transactions on Microwave Theory and Techniques*, vol. 71, no. 11, pp. 4618-4627, 2023.

[31] F. Montiel, M. Neviere, "Electromagnetic study of the diffraction of light by a mask used in photolithography", *Optics Communications*, vol. 101, no. 3, pp. 151–156, 1993.

[32] G. Granet, B. Guizal, "Analysis of strip gratings using a parametric modal method by Fourier expansions", *Optics Communications*, vol. 255, no. 1, pp. 1–11, 2005.

[33] M. Kalantari, K. Paran, "Analyzing metamaterial layer by simpler approach based on mode matching technique", *IET Microwaves, Antennas & Propagation*, vol. 11, no. 5, pp. 607-616, 2017.

[34] M. Kalantari Meybodi, K. Paran, "Straightforward analysis of the effect of any H-plane inductive diaphragm in waveguide", *IET Microwaves, Antennas & Propagation*, vol. 11, no. 5, pp. 577-583, 2017.